Hindawi
International Journal of Antennas and Propagation
Volume 2022, Article ID 9970477, 8 pages
https://doi.org/10.1155/2022/9970477

Research Article

A Dual-Band Wearable Conformal Antenna Based on Artificial Magnetic Conductor

Shuqi Wang and Huan Gao

School of Communication and Information Engineering, Xi'an University of Science and Technology, Xi'an 710054, China

Correspondence should be addressed to Shuqi Wang; wangshuqi@xust.edu.cn

Received 8 November 2021; Accepted 25 February 2022; Published 16 March 2022

Academic Editor: Giuseppe Castaldi

In order to improve the effectiveness of the antenna performance of wearable devices, a dual-band flexible monopole antenna with a 3×3 artificial magnetic conductor structure of the ISM band is proposed by using meander technology. An annular-shaped artificial magnetic conductor (AMC) is placed directly below the antenna, which can be better suitable for wireless body area network (WBAN) applications. A polyimide substance is used as the antenna substrate, which makes the antenna bendable and thin. Benefiting from the in-phase reflective properties of the double ring AMC structure, the antenna has good radiation characteristics. Compared with the single antenna, numerical simulation and measurement results show that the gain of the AMC-loaded antenna is increased by 4.54 dBi and 3.86 dBi at 2.45 GHz and 5.8 GHz, respectively. In addition, the specific absorption rate (SAR) of 1 g is only 0.35 W/kg at 2.45 GHz and 0.39 W/Kg at 5.8 GHz when the antenna is placed on human tissue, which is far below the Federal Communications Commission (FCC) standard. The antenna is easy to be conform to the human body and has strong robustness to structural deformation and human body load.

1. Introduction

Wireless body area networks are one of the important technical means for personal health information collection and transmission. With the rapid development of artificial intelligence and Internet of Things technology, low-power wearable devices have become the focus of academic and industrial circles [1–4]. The design of flexible antennas has great significance for the effective and reliable transmission of wearable device data [5–7].

Antennas for wearable devices should not only have the characteristics of softness, low profile, and small shape [8] but also need to inhibit the excessive radiation and heat absorbed by the human body [9, 10]. The United States and the European Union limit the standard value of SAR to measure the safety of antenna radiation [11]. At present, the antennas used in wearable devices mainly include monopole antennas [12], microstrip patch antennas [13], planar inverted-F antennas [14], and button antennas [15], etc. Chun Ping Deng proposed a miniascape-like triple-band monopole antenna which covers 3.1–3.3, 4.2–4.9, and 6–10.6 GHz. Its radiation efficiency is 30.3%, 45%, and 62.7% in each band for mismatching and loss close to human tissues [16]. Le and Yun proposed a very compact dual-band antenna adopting zigzag line and gap loading. The size is only $0.15 \times 0.1 \times 0.004\lambda 3$. The change of S-parameter under bending conditions can be ignored, but the gain is only 2.0 dBi and 3.2 dBi due to the influence of human tissues below, and the SAR value meets the standard only at 10 mm away from the human body [17]. Li et al. designed an ultrawideband antenna for the first time by using flexible graphite films with high conductivity as the antenna radiation element. The antenna achieved 122% fractional bandwidth from 0.34 GHz to 1.4 GHz, and the overall profile was only about 0.1 mm. Yet its near-omnidirectional radiation pattern indicates that there is a certain impact on the safety of the wearer [18].

In order to alleviate the problem of antenna impedance mismatch caused by human tissue, an electromagnetic metasurface structure has been introduced into wearable

antennas to effectively reduce the SAR value of radiation into the human body. Jiang et al. have successively designed two wearable antennas loaded with metasurface units. A medical body area network antenna operating at 2.36–2.4 GHz is proposed in [19], the metasurface under the planar monopole antenna not only serves as an isolated ground connection but also as the main radiator. A circularly polarized flexible antenna using a composite material of PDMS and silver nanowires was proposed in [20]. By placing a 2×2 cell structure below the monopole antenna, the circular polarization bandwidth is greatly increased. Compared with traditional circular polarization antennas, the antenna has better stability to structural deformation. Liu et al. studied a single-band monopole antenna integrating a small slotted Jerusalem cross artificial magnetic conductor grafting layer for telemedicine applications. Except for a 64% reduction in SAR, the front and back ratio (FB) and gain increased by 8 dB and 3.7 dBi, respectively, compared to before loading the AMC [21]. Gao et al. proposed a slot antenna with an EBG structure, which is made of felt and conductive fabric and can easily form conformal with the human body, and the FB ratio can reach 17 dB [22]. Alemaryeen and Noghanian used Pellon fabric as a substrate to manufacture a broadband antenna system with an impedance bandwidth of 34%, achieving good impedance matching in the 5.8 GHz band. It is confirmed that the performance of the integrated AMC antenna is much better than that of the traditional monopole antenna, and the radiation of the back lobe is greatly reduced, but the specific absorption rate is not discussed in detail [23]. Gao et al. designed a wearable antenna with a nonuniform metasurface by using the characteristic mode analysis. By adjusting the rotation angle of the cell, the working band of the antenna is majorized to cover the 5 GHz WLAN, and the average gain reaches 7.63 dBi, which provides a new idea for the design of nonuniform metasurface [24]. Several other papers have also proposed different topologies of metasurface wearable antennas that operate in the free and open ISM band. According to reports [25, 26], the proposed antenna has a small volume and high gain, and the antenna inspired by the structure of electromagnetic band-gap and artificial magnetic conductor is also helpful in minimizing the electromagnetic coupling between the antenna and the human body, while reducing the specific absorption rate of the human body by more than 99%.

For further exploration of the emission characteristics in body area network communication, a low-profile flexible dual-band wearable antenna based on compact AMC is proposed. The feasibility of utilizing the in-phase reflective properties of the AMC structure to suppress backward radiation, improve the radiation gain, and enhance the isolation effect between the antenna and the human body is explored.

2. Configuration of Antenna and AMC Structure

The overall structure of the funnel-shaped dual-band wearable antenna system is shown in Figure 1, which is composed of a top monopole antenna and an AMC array below. The above antenna consists of three layers, and the funnel-shaped radiation unit in the upper layer generates high-frequency signals. Then a rectangular slot of length L_2 and width W_2 is placed in the middle of the patch to achieve miniaturization. A new low-frequency resonance point is introduced by meander technology, that is, the gap etched on the backside of the floor. For the sake of increasing the flexibility and radiation performance of the antenna, the substrate is made of flexible polyimide material with a relative dielectric constant of 3.5 and a thickness of 0.5 mm. The 1.15 mm wide 50Ω impedance feeder is used to match the input impedance without an additional matching network.

Three-dimensional electromagnetic simulation software, CST, was used for simulation. All the optimized parameters are $L = 30$ mm, $W = 23$ mm, $L_1 = 13.2$ mm, $W_1 = 6.4$ mm, $L_2 = 8.1$ mm, $W_2 = 1.65$ mm, $L_3 = 11$ mm, $W_3 = 1.15$ mm, $t = 1.8$ mm, $h = 11.1$ mm, $u = 0.6$ mm, $a_1 = 8.5$ mm, $a_2 = 8.3$ mm, and $a_3 = 4.1$ mm.

The frequency selection surface design uses a 3×3 double-annular AMC structure. Its structure is simple and its unit volume is $D_0 \times D_0 \times 1.2\ \text{mm}^3$. And the equivalent circuit diagram of the square annular AMC unit is shown in Figure 2, C_1 represents the equivalent capacitance between the upper patch and the ground, C_2 represents the surface capacitance caused by the element gap, and L_S is the equivalent inductance generated by the current resonance on the surface of the patch.

Input impedance $Z_0(\omega)$ and resonant frequency f_0 are determined by the following equation:

$$Z_0(\omega) = Z_1(\omega) \| Z_2(\omega) = \frac{j\left(1 - \omega^2 C_1 L_s\right)}{\omega\left(C_1 C_2 L_s \omega^2 - C_1 - C_2\right)},$$
$$f_0 = \frac{1}{2\pi}\sqrt{\frac{C_1 + C_2}{C_1 C_2 L_s}}. \quad (1)$$

The reflection phases of the double-annular AMC structure and the solid patch structure are shown in Figure 3.

The material, thickness, and sizes of the two structures remain the same, and the size of the patch structure is larger than that of the ring structure at the same resonant frequency. Let us adjust the edge length of the ring cell so that it produces two 0° reflected phase points, and the AMC reflected phase is approximately consistent with 2.45 GHz and 5.8 GHz. The optimized size parameters are $D_0 = 20.4$ mm, $D_1 = 18.8$ mm, $D_2 = 9.4$ mm, and $g = 1$ mm. The simulation results indicate that increasing the element gap will increase the resonance frequency of each band, while increasing the ring edge length will decrease the resonance point of the corresponding band. The whole structure is composed of three layers. Besides the antenna and AMC surface designed previously, there is also a flexible foam layer in the middle. The antenna prototype made is shown in Figure 4.

3. Analysis of Simulation and Measurement Results

3.1. S-Parameters in Different Cases. The measured and simulated S_{11} curve of the antenna are shown in Figure 5, and a comparison is made between the structures with and

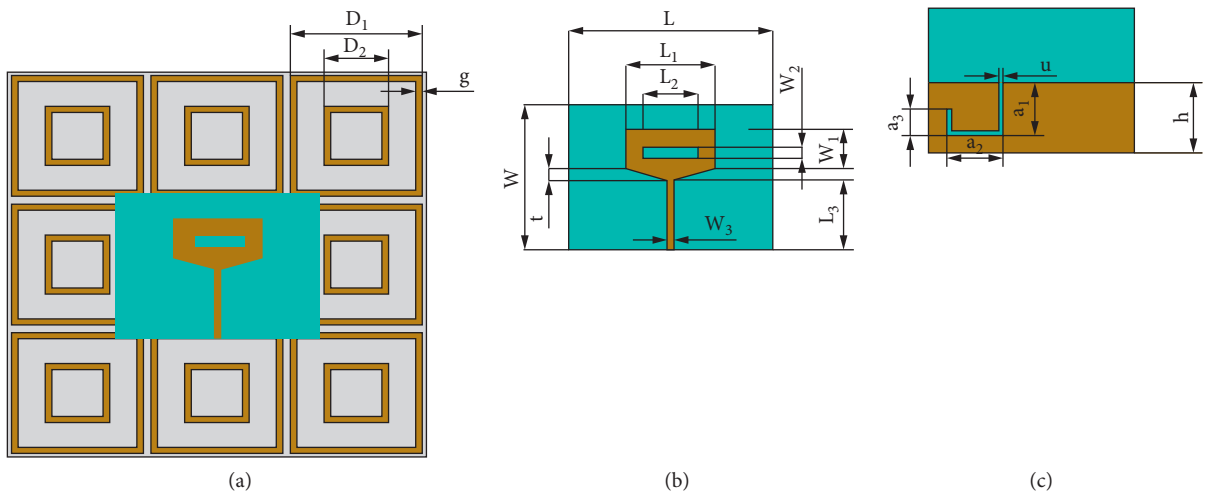

Figure 1: Configuration of the funnel-shaped antenna system: (a) global view, (b) front view, and (c) back view.

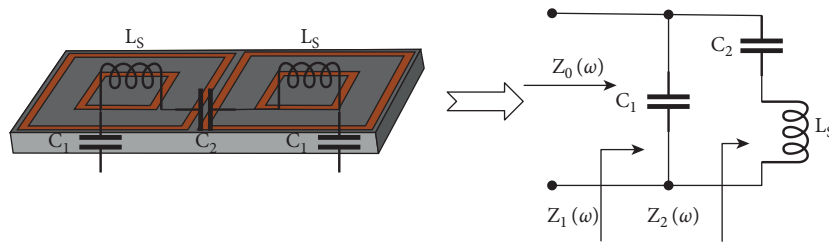

Figure 2: Equivalent circuit model of the AMC.

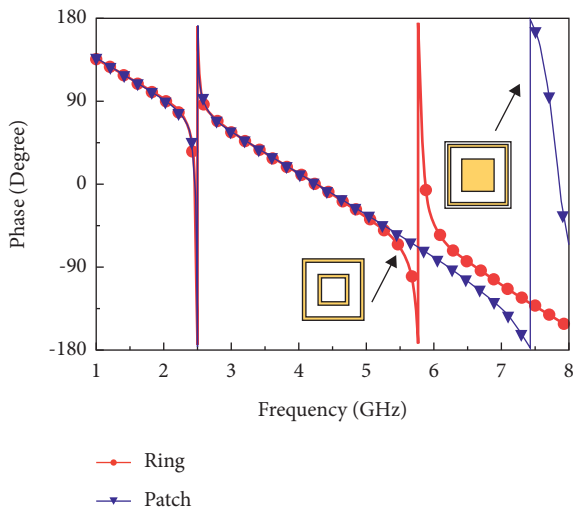

Figure 3: Reflection phase of the square ring and square patch.

without AMC. The antenna still has dual-band characteristics after being integrated with the AMC structure, the resonance points less than −10 dB are produced at 2.45 GHz and 5.8 GHz. The measured S_{11} is in accordance well with the simulated results. Compared with the antenna without AMC structure, the bandwidth of the antenna is narrower, which may be caused by the narrow reflection phase bandgap of the periodic structure. But it can also cover the 2.4 GHz–2.485 GHz and 5.725 GHz–5.85 GHz bands of the wearable antenna, which shows that the designed antenna meets the index requirements.

To reflect the actual operation scene, the designed antenna system is placed on the human abdomen to demonstrate the influence of human tissues on its impedance matching. Measurement S_{11} of the antenna approaching human tissues is shown in Figure 6. It can be perceived that after the AMC structure is loaded, the frequency point is somewhat offset. But in general, the electrical characteristics of the human body have little effect on the antenna's performance. This, on account of the in-phase reflective properties of the artificial magnetic conductor, effectively isolates the antenna from the human body.

For the sake of investigating the wearable performance of the antenna further, the *S*-parameter curves when the foam cylinder bent at different radii are shown in Figure 7. As the bending radius R continues to decrease, the low-frequency band moves to the left, and the impedance matching gradually gets worse. However, the bandwidth of $S_{11} < -10$ dB can basically cover the ISM band. In other words, the bending condition has little effect on the antenna performance, which can be applied to wearable devices.

3.2. Far-Field Radiation Patterns, Gain, and Efficiency. An antenna pattern is a graph that represents the relationship between antenna radiation characteristics and

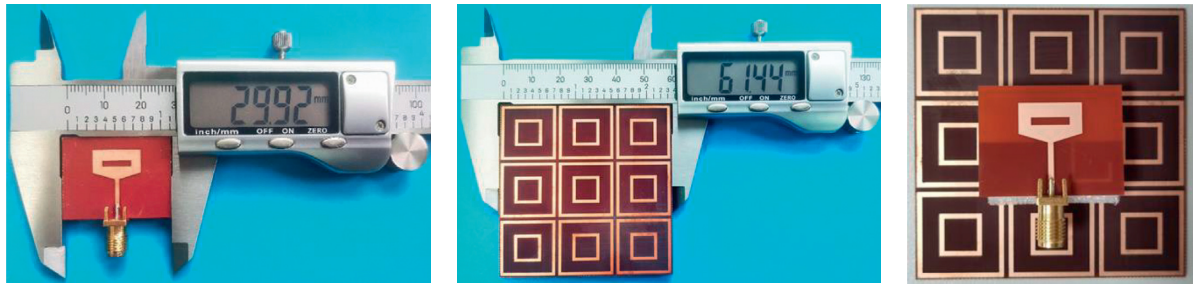

Figure 4: Photographs of the antenna system: (a) monopole antenna, (b) AMC surface, and (c) assembled antenna system.

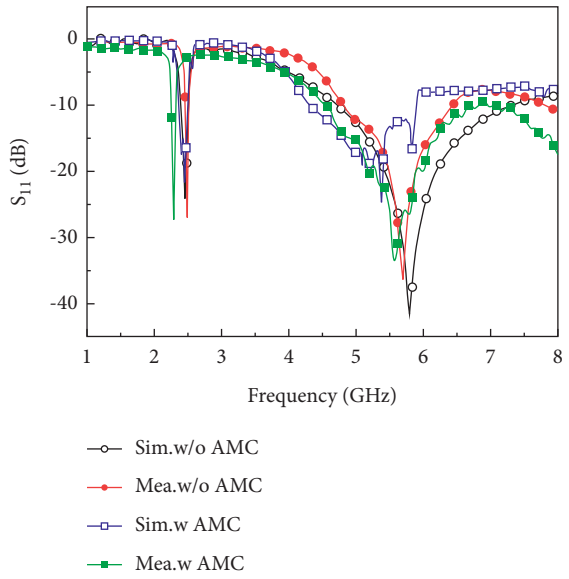

Figure 5: Simulated and measured S_{11} for the funnel-shaped antenna with and without AMC.

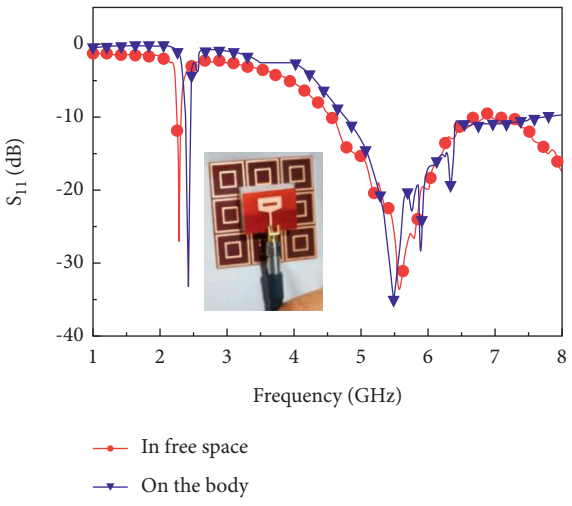

Figure 6: Measured S_{11} on human tissues for the proposed antenna system.

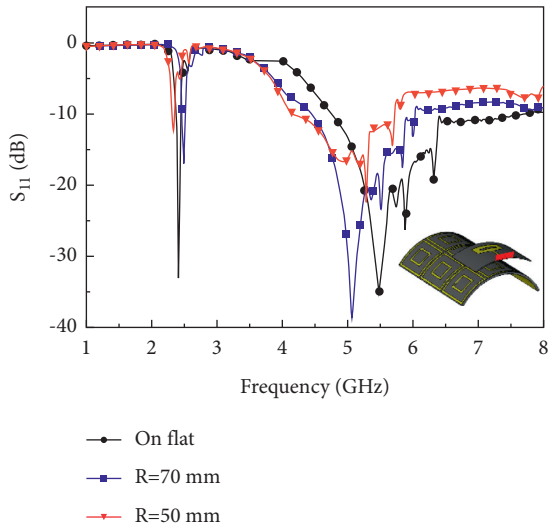

Figure 7: S_{11} of the proposed antenna system when bent under different radius.

spatial angle. The normalized radiation patterns of 2.45 GHz and 5.8 GHz are shown in Figure 8, which includes simulation and measurement results. The pattern of the YOZ plane of a monopole antenna is symmetrical, while the radiation of the XOZ plane is omnidirectional. After the antenna is loaded with the AMC structure, the amplitude of the back lobe of the whole antenna is significantly reduced compared with that of the main lobe, and the maximum radiation direction of the main lobe is kept in the Z-axis direction of the antenna, thereby obtaining a better orientation. This also implies that the antenna leads to low-back radiation toward the human body with the inclusion of AMC, which is in line with the unilateral radiation direction required by the design of the wearable device. The measured results are consistent with the simulation results at the two frequency points. The difference between them is due to manufacturing and measurement errors.

Besides, the gain and efficiency of the antenna are shown in Figure 9. It can be obtained that the gain at both frequency bands is significantly improved when the AMC structure is

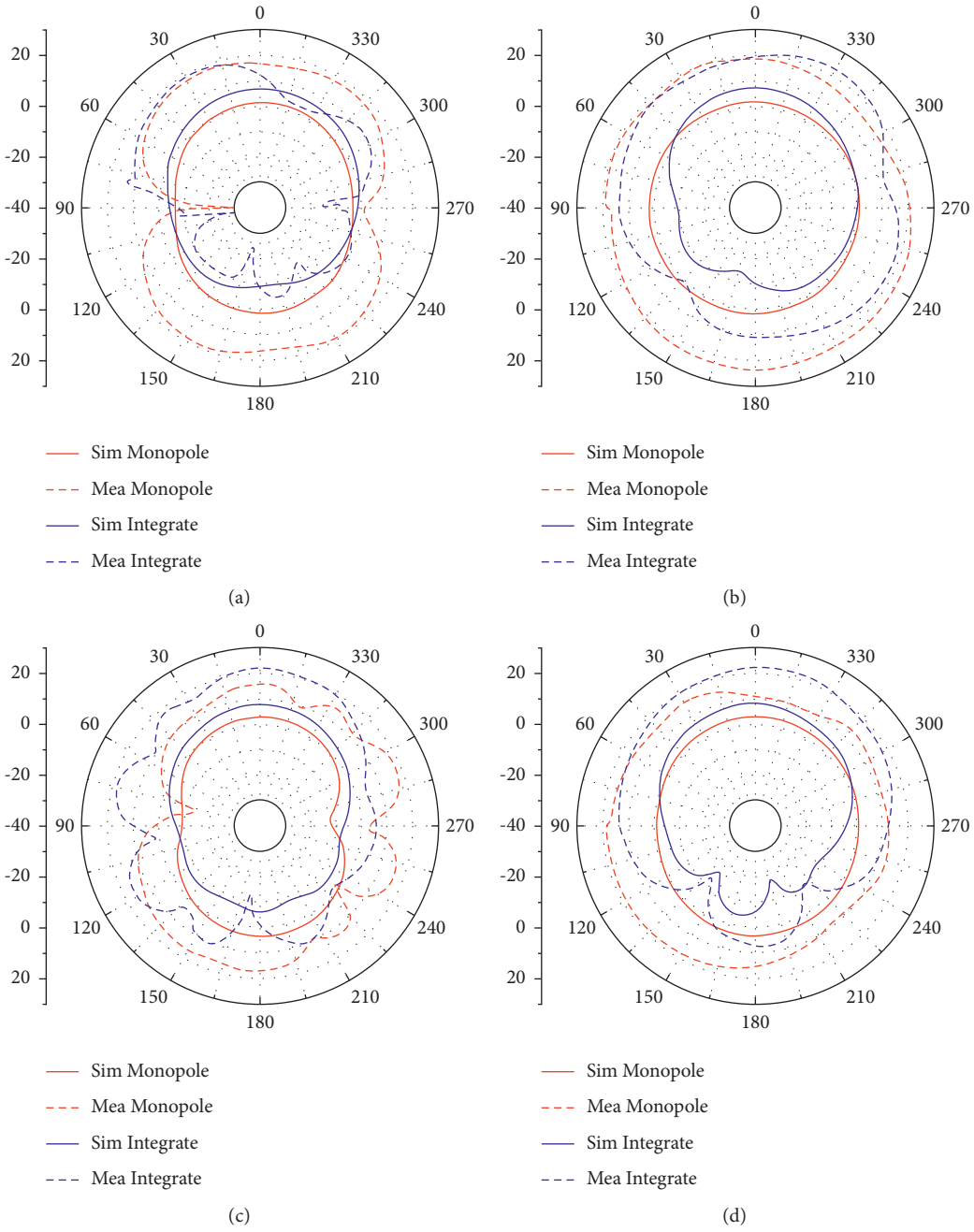

Figure 8: Radiation pattern of antenna: (a) 2.45 GHz in E-plane, (b) 2.45 GHz in H-plane, (c) 5.8 GHz in E-plane, and (d) 5.8 GHz in H-plane.

used as an antenna reflector. Among them, it increases from 1.13 dBi to 5.67 dBi at 2.45 GHz and from 3.03 dBi to 6.89 dBi at 5.8 GHz. On the contrary, the propagation path of electromagnetic waves between the top antenna and the AMC structure becomes longer and the power loss increases due to the addition of the AMC array [27]. So, the efficiency also decreases by about 10%.

4. SAR Value

SAR is an important parameter to evaluate the radiation safety performance of antennas. A three layer model of human tissues with skin, fat, and muscle [28] was used to analyze the SAR of the antenna. The relative permittivity, electrical conductivity, and tissue density of each layer of

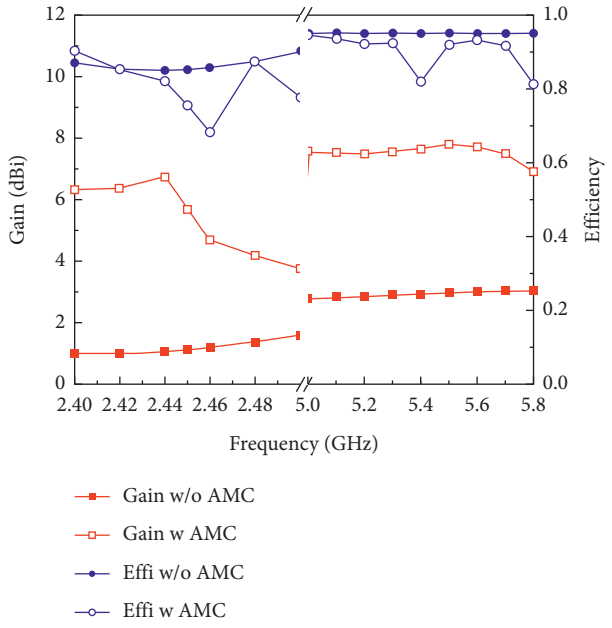

Figure 9: The gain and efficiency of the antenna.

Table 1: Electromagnetic parameters of human tissues.

Tissue	Relative permittivity	Conductivity (S/m)	Density (kg/m^3)
Skin	38.01	1.46	1001
Fat	5.28	0.10	900
Muscle	52.73	1.76	1006

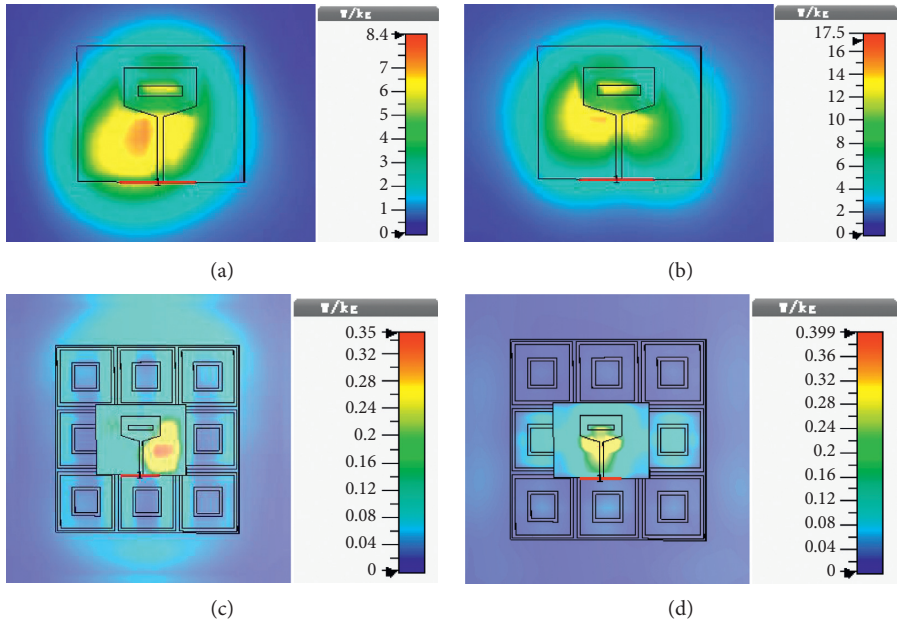

Figure 10: SAR value distribution of antenna: (a) monopole at 2.45 GHz, (b) monopole at 5.8 GHz, (c) integrate at 2.45 GHz, and (d) integrate at 5.8 GHz.

Table 2: Comparison of the proposed antenna with other antennas reported in the literature.

Ref.	Dimensions (mm^2)	Number of unit cell	Freq. (GHz)	SAR value 1 g (W/kg)	Distance from body (mm)	Gain (dBi)
[9]	72×72	3×3	2.45/5.8	2.48/3.33	—	5.2/7.7
[10]	86×86	4×4	3.5/5.8	0.0683/0.333	1	9.07/6.63
[12]	68×38	2×1	2.45	0.5	2	6.88
[19]	62×42	2×2	2.4	0.48	5	6.2
[22]	81×81	3×3	2.45	0.554	6	7.3
[25]	75.7×75.7	3×3	2.45	0.022	3	6.58
This paper	61.5×61.5	3×3	2.45/5.8	0.35/0.39	1	5.67/6.89

human tissue are shown in Table 1. Here we refer to the tissue thickness of ordinary adults, that is, the skin layer thickness is 1 mm, the fat layer thickness is 2 mm, and the muscle layer thickness is 10 mm for simulation calculation. The antenna with and without the AMC structure is located 1 mm above the human tissue model, and the simulation model and results are shown in Figure 10.

The maximum SAR of the proposed antenna is 0.35 and 0.39 W/kg at 2.45 GHz and 5.8 GHz, respectively, which is far below the standard of less than 1.6 W/kg for 1 g of tissue. It can meet the performance indicators of a wearable antenna in terms of security. Compared with the monopole antenna, the AMC structure significantly reduces the SAR value. Last but not least, Table 2 lists the comparison between the proposed antenna in this paper and some other recent related references in human body performance. An analogy was drawn with respect to the physical dimensions of antenna and its resonant frequency. Meanwhile, it also includes several other important indicators of the antenna.

5. Conclusions

In conclusion, a monopole antenna with a compact 3×3 artificial magnetic conductor structure is designed for WBAN application, which achieves good impedance matching in the ISM band. The antenna system has the advantages of being small size, simple structure, and good stability. In addition, the antenna can maintain dual-band resonance both in free space and near the human body. The gain is significantly improved to 5.67 dBi and 6.89 dBi in 2.45 GHz and 5.8 GHz, respectively, while the isolation between the antenna and the human body can be enhanced and the bending condition has little effect on the antenna performance. The fabricated antenna works stably on human tissue. The maximum SAR is 0.35 and 0.39 W/kg in 2.45 GHz and 5.8 GHz, respectively, which is far below the FCC standard of less than 1.6 W/kg for 1 g of tissue. The scheme verifies the feasibility of using the in-phase reflection characteristics of the AMC structure to improve the antenna performance and applies it to the design of flexible antennas for medical applications.

Data Availability

The data of the manuscript could be obtained through email: wangshuqi@xust.edu.cn.

Conflicts of Interest

The authors declare that they have no conflicts of interest.

Acknowledgments

This work was supported by the National Natural Science Foundation of China (NFSC) under grant no. 61901357.

References

[1] S. Movassaghi, M. Abolhasan, J. Lipman, D. Smith, and A. Jamalipour, "Wireless body area networks: a survey," *IEEE Communications Surveys & Tutorials*, vol. 16, no. 3, pp. 1658–1686, 2014.

[2] M. El Gharbi, R. Fernández-García, S. Ahyoud, and I. Gil, "A review of flexible wearable antenna sensors: design, fabrication methods, and applications," *Materials*, vol. 13, no. 17, pp. 1–18, 2020.

[3] B. Almohammed, A. Ismail, and A. Sali, "Electro-textile wearable antennas in wireless body area networks: materials, antenna design, manufacturing techniques, and human body consideration—a review," *Textile Research Journal*, vol. 91, no. 5–6, pp. 646–663, 2021.

[4] A. Y. I. Ashyap, Z. Zainal Abidin, S. H. Dahlan, H. A. Majid, and G. Saleh, "Metamaterial inspired fabric antenna for wearable applications," *International Journal RF Microwords Computer Engineering*, vol. 29, no. 3, pp. 1–10, 2019.

[5] K. Zhang, G. A. E. Vandenbosch, and S. Yan, "A novel design approach for compact wearable antennas based on metasurfaces," *IEEE Transactions on Biomedical Circuits and Systems*, vol. 14, no. 4, pp. 918–927, 2020.

[6] A. Veeraselvam, G. N. A. Mohammed, K. Savarimuthu, M. Marimuthu, and B. Balasubramanian, "Polarization diversity enabled flexible directional UWB monopole antenna for WBAN communications," *Int. J. RF Microsoft word. Computer. Engineering*, vol. 30, pp. 1–12, 2020.

[7] A. S. M. Alqadami, K. S. Bialkowski, A. T. Mobashsher, and A. M. Abbosh, "Wearable electromagnetic head imaging system using flexible wideband Antenna array based on polymer technology for brain stroke diagnosis," *IEEE Transactions on Biomedical Circuits and Systems*, vol. 13, no. 1, pp. 124–134, 2019.

[8] K. Zhang, P. Jack Soh, and S. Yan, "Meta wearable antennas-a review of metamaterial based antennas in wireless body area networks," *Materials*, vol. 14, no. 1, pp. 1–20, 2021.

[9] M. Wang, Z. Yang, J. Wu et al., "Investigation of SAR reduction using flexible antenna with metamaterial structure in wireless body area network," *IEEE Transactions on Antennas and Propagation*, vol. 66, no. 6, pp. 3076–3086, 2018.

[10] M. El Atrash, M. A. Abdalla, and H. M. Elhennawy, "A wearable dual-band low profile high gain low SAR antenna AMC-backed for WBAN applications," *IEEE Transactions on Antennas and Propagation*, vol. 67, no. 10, pp. 6378–6388, 2019.

[11] I. S. C. C. 28 IEEE standards coordinating committee, "I. S. C. C. 28 IEEE standards coordination commite," *IEEE Recommended Practice for Measurements and Computations of Radio Frequency Electromagnetic Fields with Respect to Human Exposure to Such Fields*, vol. 2002, 2003.

[12] M. A. B. Abbasi, S. S. Nikolaou, M. A. Antoniades, M. Nikolic Stevanovic, and P. Vryonides, "Compact EBG-backed planar monopole for BAN wearable applications," *IEEE Transactions on Antennas and Propagation*, vol. 65, no. 2, pp. 453–463, 2017.

[13] C. Mendes and C. Peixeiro, "A dual-mode single-band wearable microstrip antenna for body area networks," *IEEE Antennas and Wireless Propagation Letters*, vol. 16, pp. 3055–3058, 2017.

[14] G.-P. Gao, C. Yang, B. Hu, R.-F. Zhang, and S.-F. Wang, "A wide-bandwidth wearable all-textile PIFA with dual resonance modes for 5 GHz WLAN applications," *IEEE Transactions on Antennas and Propagation*, vol. 67, no. 6, pp. 4206–4211, 2019.

[15] X. Y. Zhang, H. Wong, T. Mo, and Y. F. Cao, "Dual-band dual-mode button antenna for on-body and off-body communications," *IEEE Transactions on Biomedical Circuits and Systems*, vol. 11, no. 4, pp. 933–941, 2017.

[16] C. P. Chun-Ping Deng, X. Y. Xiong-Ying Liu, Z. K. Zhen-Kun Zhang, and M. M. Tentzeris, "A miniascape-like triple-band monopole antenna for WBAN applications," *IEEE Antennas and Wireless Propagation Letters*, vol. 11, pp. 1330–1333, 2012.

[17] T. T. Le and T.-Y. Yun, "Miniaturization of a dual-band wearable antenna for WBAN applications," *IEEE Antennas and Wireless Propagation Letters*, vol. 19, no. 8, pp. 1452–1456, 2020.

[18] W. Li, H. Zu, J. Liu, and B. Wu, "A low-profile ultrawideband Antenna based on flexible graphite films for on-body wearable applications," *Materials*, vol. 14, no. 16, p. 4526, 2021.

[19] Z. H. Jiang, D. E. Brocker, P. E. Sieber, and D. H. Werner, "A compact, low-profile metasurface-enabled antenna for wearable medical body-area network devices," *IEEE Transactions on Antennas and Propagation*, vol. 62, no. 8, pp. 4021–4030, 2014.

[20] Z. H. Jiang, Z. Cui, T. Yue, Y. Zhu, and D. H. Werner, "Compact, highly efficient, and fully flexible circularly polarized antenna enabled by silver nanowires for wireless body-area networks," *IEEE Transactions on Biomedical Circuits and Systems*, vol. 11, no. 4, pp. 920–932, 2017.

[21] H. Liu, J. Wang, and X. Luo, "Flexible and compact AMC based antenna for WBAN applications," in *Proceedings of the 2017 IEEE Antennas Propagation Society International Symposium*, pp. 587-588, San Diego, CA, USA, January 2017.

[22] G.-P. Gao, B. Hu, S.-F. Wang, and C. Yang, "Wearable circular ring slot antenna with EBG structure for wireless body area network," *IEEE Antennas and Wireless Propagation Letters*, vol. 17, no. 3, pp. 434–437, 2018.

[23] A. Alemaryeen and S. Noghanian, "On-body low-profile textile antenna with artificial magnetic conductor," *IEEE Transactions on Antennas and Propagation*, vol. 67, no. 6, pp. 3649–3656, 2019.

[24] G. Gao, R.-F. Zhang, W.-F. Geng, H.-J. Meng, and B. Hu, "Characteristic mode analysis of a nonuniform metasurface antenna for wearable applications," *IEEE Antennas and Wireless Propagation Letters*, vol. 19, no. 8, pp. 1355–1359, 2020.

[25] M. El Atrash, O. F. Abdalgalil, I. S. Mahmoud, M. A. Abdalla, and S. R. Zahran, "Wearable high gain low SAR antenna loaded with backed all textile EBG for WBAN applications," *IET Microwaves, Antennas & Propagation*, vol. 14, no. 8, pp. 791–799, 2020.

[26] N. Ramanpreet, M. Rattan, and S. S. Gill, "Compact and low profile planar antenna with novel metastructure for wearable MBAN devices," *Wireless Personal Communications*, vol. 118, no. 4, pp. 3335–3347, 2021.

[27] G. Gao, R. Zhang, C. Yang, H. Meng, W. Geng, and B. Hu, "Microstrip monopole antenna with a novel UC-EBG for 2.4 GHz WBAN applications," *IET Microwaves, Antennas & Propagation*, vol. 13, no. 13, pp. 2319–2323, 2019.

[28] J. Gemio, J. Parron, and J. Soler, "Human body effects on implantable antennas for ism bands applications: models comparison and propagation losses study," *Progress In Electromagnetics Research*, vol. 110, pp. 437–452, 2010.